HHS Public Access

Author manuscript

J Neuroimaging. Author manuscript; available in PMC 2023 January 01.

Published in final edited form as:

J Neuroimaging. 2022 January ; 32(1): 68–79. doi:10.1111/jon.12929.

"Super-Resolution Reconstruction of T2-Weighted Thick Slice Neonatal Brain MRI Scans"

Nurten C. Askin Incebacak[1], **Yao Sui, PhD**[2], **Laura Gui Levy, PhD**[3], **Laura Merlini, MD**[4], **Joana Sa de Almeida, MD PhD**[3], **Sebastien Courvoisier, PhD**[1,5], **Tess E. Wallace, PhD**[2], **Antoine Klauser, PhD**[1,5], **Onur Afacan, PhD**[2], **Simon K. Warfield, PhD**[2], **Petra Hüppi, MD**[3], **Francois Lazeyras, PhD**[1,5]

[1]Department of Radiology and Medical Informatics, University of Geneva, Geneva, Switzerland

[2]CRL, Department of Radiology, Boston Children's Hospital, Harvard Medical School, Boston, Massachusetts

[3]Division of Development and Growth, Department of Woman, Child and Adolescent, University Hospitals of Geneva, Geneva, Switzerland

[4]Pediatric Radiology Unit, Division of Radiology, University Hospitals of Geneva, Geneva, Switzerland

[5]CIBM, Center of Biomedical Imaging, Geneva, Switzerland

Abstract

BACKGROUND AND PURPOSE: Super-resolution reconstruction (SRR) can be used to reconstruct 3D high-resolution (HR) volume from several 2D low-resolution (LR) stacks of MRI slices. The purpose is to compare lengthy 2D T2-weighted HR image acquisition of neonatal subjects with 3D SR reconstruction from several LR stacks in terms of image quality for clinical and morphometric assessments.

METHODS: LR brain images were acquired from neonatal subjects to reconstruct isotropic 3D HR volumes by using SRR algorithm. Quality assessments were done by an experienced pediatric radiologist using scoring criteria adapted to newborn anatomical landmarks. The Wilcoxon Signed-Rank test was used to compare scoring results between HR and SRR images. For quantitative assessments, morphology-based segmentation was performed on both HR and SRR images and Dice coefficients between the results were computed. Additionally, simple linear regression was performed to compare the tissue volumes.

RESULTS: No statistical difference was found between HR and SRR structural scores using Wilcoxon Signed-Rank test ($p=0.63$, $Z=0.48$). Regarding segmentation results, R^2 values for the volumes of gray matter, white matter, cerebrospinal fluid, basal ganglia, cerebellum and total brain volume including brain stem ranged between 0.95-0.99. Dice coefficients between the segmented regions from HR and SRR ranged between 0.83±0.04 and 0.96±0.01.

Corresponding Author Info: Nurten Ceren Askin Incebacak, Radiology-CIBM, HUG, 4 Gabrielle-Perret-Gentil, 1205, Geneva, Switzerland, Contact number: +41 (0) 22 372 33 11, nurtenceren.askin@unige.ch.

CONCLUSION: Qualitative and quantitative assessments showed that 3D SRR of several LR images produces images that are comparable quality to standard 2D HR image acquisition for healthy neonatal imaging without loss of anatomical details with similar edge definition allowing the detection of fine anatomical structures and permitting comparable morphometric measurement.

Keywords

super-resolution; T2-weighted; neonatal brain MRI; mitigate motion; segmentation

Introduction

Prematurity and neonatal brain injuries are important risk factors for developmental abnormalities[1] that might result in long-term neurodevelopmental impairments with an impact in both childhood and adulthood.[2,3] MRI is commonly used for clinical diagnostic purposes and is suitable for the assessment of early brain development in pediatric imaging.[4] The analysis and characterization of early brain development using MRI have increased over the years.[5-7] In newborn imaging, T2-weighted high-resolution (HR) MRI is typically used, because it provides the best gray-white matter contrast in the pre-myelinated neonatal brain for clinical diagnosis and morphometric purposes, such as brain segmentation, whereas T1-weighted imaging is mainly used to visualize the myelination process.[8]

Subject motion is a limitation for acquiring good contrast and high-quality images, which is especially challenging for uncooperative subjects like infants. In clinics, sedation or general anesthesia can be used to circumvent motion however in research settings it is not possible due to ethical considerations Therefore, there is a strong need for new techniques to circumvent motion in order to improve image quality and prevent unnecessary reacquisition of motion-corrupted images. Several methods have been developed to overcome the subject motion problem including parallel imaging and robust k-space sampling.[9,10]

One approach is to split the lengthy high-resolution acquisitions into several fast low-resolution (LR) scans and to combine the images to reconstruct a final 3D volume using super-resolution (SR) algorithms.[11] The main advantage of this approach is the avoidance of additional hardware requirements, in contrast to the other existing techniques, and the minimization of the reacquisition time in the case of a corrupted scan.

Super-resolution reconstruction (SRR) has been widely used in image processing[12] and recently adapted to MRI taking advantage of the capability of controlling slice thickness, acquisition speed and orientation, in order to achieve the desired image resolution.[13,14] In SRR, to improve the resolution efficiently, new information needs to be added, which is generally done by subpixel translation or rotation. In MRI, this can be achieved by either acquiring anisotropic voxels in a different orientation or by shifting the field-of-view. Among recent studies of SRR on fetal and neonatal MRI,[11,15-20] Rousseau et al. proposed an algorithm where three orthogonal MRI volumes were acquired and slice-to-volume registration was applied before reconstructing the high-resolution volume.[16] Later, Gholipour et al. proposed an explicit model of MR image formation, and showed how multiple observations could be used to determine the unobserved high-resolution data using a forward model of the observed LR data.[17] They applied their model to pediatric and fetal

MR images. The acquisition of thick slices has led to a reduction of the image acquisition time and thus reduces the risk of motion artifacts.

In this study, we used an SRR method for obtaining 3D high-resolution MRI volumes with good contrast and sharp edges from healthy neonatal infant brains. SRR volumes were reconstructed using a multi-scale gradient field prior from several orthogonal 2D T2-weighted low-resolution MR stacks based on the recent work by Sui et al.[21] We assessed the quality of the final SRR compared to the standard HR image in two ways: 1) comparison of the segmentation results from both images and 2) fine structures visibility scoring by a pediatric radiologist. The selected structures are considered to play an important role in the assessment of early brain development.

Methods

Subjects

The population assessed in this study has been recruited at the neonatal and maternity units from 2017 to 2020, as part of a research study which aims assessing the impact of prematurity on early brain development. Full-term (FT) newborns (n=23), with a gestational age (GA) at birth between 37-41 weeks, were scanned 2-3 days after birth (between 39-41 weeks GA). Preterm infants (n=45), born between 24-32 weeks GA, were scanned twice: soon after birth, namely preterm at birth (PTB) between 33-34 weeks GA and at term equivalent age (TEA), between 39-41 weeks GA. Research Ethics Committee approval was granted for the study and written parental consent was obtained prior to infants' participation in the study.

Imaging Protocol

All examinations were performed on a 3T MRI scanner (Prisma, Siemens, Erlangen, Germany) with a 16-channel receiver neonatal head coil (LMT medical systems, Lübeck, Germany). None of the newborns received sedation or general anesthesia during the examination. Subject motions were limited by wrapping babies and using air pillows. For the standard high-resolution 2D T2-weighted (T2w) image, the turbo spin echo (TSE) sequence was used (coronal slices covering the whole brain, repetition time [TR] = 4990 ms, echo time [TE] = 160 ms, echo train length [ETL]= 15, flip angle [FA] = 150°, concatenation (number of stacks) 6, acquisition time [TA] = 5 min and spatial resolution = 0.8x0.8x1.2 mm^3).

For super-resolution reconstruction three orthogonal (coronal, sagittal, axial) low resolution 2D T2w TSE images were acquired from 35 neonatal subjects including FT (n=5), PTB (n=10) and TEA (n=20). LR images of 28 subjects were acquired with the following parameters: TR = 7470 ms, TE = 157 ms, ETL= 9, TA = 1.14 min for single LR acquisition, yielding total TA = 3.42 min, FA = 150°, concatenation 1, with in-plane resolution of 0.8x0.8mm and through-plane resolution of 3 mm. LR images of 7 subjects were acquired with following parameters: TR = 10000 ms, TE = 92 ms, ETL= 9, TA = 1.20 min, FA = 150°, concatenation 1, with in-plane resolution of 0.6x0.6mm and through-plane resolution of 2 mm. A phantom dataset was acquired from an ACR phantom using the TSE sequence

with the same imaging and reconstruction protocols for the validation of the SRR algorithm. LR images of the phantom were acquired with in-plane resolution 0.8x0.8mm and through-plane resolution of 3 mm.

Theory

SRR algorithms can be classified either as forward-based or as learning-based method. In the present work we used a forward-based model SRR, which relies on the physics of the image acquisition system.[12] In MRI, it is based on a linear acquisition model, $Y_k = D_k P_k T_k \chi + v_k$; k = 1,…, N where Y_k is LR stacks (the resolution of through-plane is often lower than in-plane) and N is the number of LR stacks, D_k is the down-sampling operator (through-plane direction), P is the point spread function (PSF), T_k is a geometric transformation between the stacks, χ denotes the SR volume to be estimated from LR images. Because SRR is an ill-posed problem, regularization is often incorporated to isolate the desired solution from indefinitely many feasible solutions. A maximum a posteriori (MAP) approach is thus leveraged to solve the SRR, $\hat{\chi}_{MAP} \coloneqq \text{argmin}\left[\sum_{k=1}^{N} \|Y_k - D_k P_k T_k \chi\|^2 + \lambda\phi(\chi)\right]$, where $\phi(\chi)$ denotes the prior that is implemented as the regularization, and λ is a balancing parameter between the data fidelity and regularization. L_2 norm minimizes the error while the regularization improves the edges in the reconstructed SR image. In this study, a multi-scale gradient field prior, as proposed previously,[21] was used to guide both spatial smoothness and edge preservation in multiple scales during the iterations of the optimization.

The multi-scale gradient field prior can be formulated as $\min_\chi \sum_{k=1}^{N} \|Y_k - D_k P_k T_k \chi\|^2 + \lambda \sum_{s=1}^{S} \|\nabla_s \chi - g_\tau(\nabla_s \chi')\|_1$ where g function (see definition in Figure1.) enhances the sharpness of large edges, while penalizing gradient perturbations (thus imposing smoothness), τ is a (non-negative) constant that balances gradient enhancement and smoothing of perturbations. Note that, the blurring operator (P) from the data fidelity results in inaccurate edge localization therefore, to improve edge definition, gradients need to be computed at multiple scales and update the SR estimation during the optimization.

SRR implementation

Multi-scale gradient prior regularization combined with super-resolution algorithm was used to reconstruct a high-resolution volume from three mutually orthogonal LR images of each neonatal subject (n=35 subjects). All the steps in SR reconstruction were implemented using MATLAB, version R2017a (MathWorks, Natick, MA). Super-resolution reconstruction procedure took about 10 minutes per subject using MacBook Pro, 2017 (Processor: 2.9 GHz Intel Core i7, Memory: 16 GB).

PSF in the through-plane direction can be inferred from slice-select excitation profile.[22] Therefore, the slice profile used in this algorithm was measured from a phantom by modifying the TSE sequence such that the readout is placed in the slice direction.[23] The slice profile measured was a Gaussian function as confirmed in literature[15-21] with a full

width half maximum equal to the slice thickness which was chosen as PSF throughout the processing.

The geometrical transformation matrix (T_k) for each LR stack was obtained using the image orientation and image position patient information from the DICOM metadata. Each LR stack was rigidly registered to the reference stack to correct for inter-volume displacements using mutual information based registration method.[24] The average of the registered images provided the initial estimation of the reconstructed SR volume. The iteration process is illustrated with a flowchart in Figure 1.

The gradient likelihood block (G_k) represents the comparison of each acquired LR image (Y_k) versus the geometrically transformed (T_k), convolved with PSF and down-sampled (D_k) current estimation of the SR volume (X_n). According to the least squares solution of L_2 norm, X_n was updated by applying the adjoint operators to the gradient image.

The regularization block ($R_{\alpha, \beta, \gamma}$), compares the n^{th} iteration of the SR estimate (X_n) with the multi-scale gradient prior shifted of itself (α, β, and γ voxels in x, y, and z directions respectively). The following parameters were chosen to finalize the reconstruction, η is the adaptive step size which varies between [0.8, 0.01] according to iteration process, whereas λ=0.05, τ=0.065, ω=0.6 and p=2 are fixed as suggested in previous work.[21] Gradient descent optimization was used to find the final high-resolution image, SRR, with a convergence criterion (root mean square error between two iterations < 1e-6).

Segmentation

The neonatal brain has different MRI tissue contrasts compared to the adult brain due to the ongoing myelination process. Therefore, automatic segmentation tools for adult brains are not suitable for neonatal brain images. Existing neonatal brain segmentation tools either rely on manual interaction or the use of atlases. In this study, an automatic segmentation method based on mathematical morphology was used, which does not rely on any manual interaction or the use of an atlas or template.[8] The method was used to segment both SRR and HR images on a subset of subjects having good quality images in both acquisitions (n=10).The following brain tissues/structures were segmented: gray matter (GM), white matter (WM), cerebrospinal fluid (CSF), basal ganglia (BG), cerebellum (Crb), and brainstem (BS).

Quality assessments of standard HR images

Image quality assessment was done visually by considering the criteria of image continuity on orthogonal reconstruction. Figure 2 displays three examples of T2w HR images: severe (top row) and mild (middle row) motion corrupted, and lastly no motion artifact (bottom row) images. Statistics on quality assessment were done on the total HR data (n=113 images). In the case of subject motion, HR sequence acquisitions could be repeated once or twice. Therefore, success rates of getting good quality HR image at multiple scan were included in the statistics.

Visibility of fine anatomical structures on HR and SRR images

In order to score the diagnostic value of SRR in comparison to standard HR images, an experienced pediatric radiologist was blinded toward which image (HR vs SRR) was reviewing (n=18, subjects with severe motion artifacts were discarded). The landmarks chosen to be scored are part of the scoring systems regarding cerebral maturation validated in the literature, visible on T2-weighted sequences and present both in preterm at TEA and in FT infants. These landmarks are described in detail by Pittet et al.,[25] and include the periventricular bands of migration, germinal matrix over the head of the caudate nucleus, crossroads 2 and 5, von Monakow segments II and linear subplate compartment along the Sylvian scissure (Figure 3). Each of them was rated with a 3-point scale value: 0 (non-visible), 1 (visible but with limitation) and 2 (well visible) on a coronal plane. Furthermore, to assess the visibility of cortical folding we scored with the same criteria the hippocampus aspect on the coronal view (Fig 3. e, e*). To score the visibility of myelination we evaluated the posterior limb of the internal capsule (PLIC) which is a milestone of cerebral maturation for both preterm at TEA and FT newborns and should be viewed as a hypointense linear structure on T2w axial planes. Figure 3 displays the fine structures denoted with arrows on the standard HR (Fig.3A) and SRR (Fig.3B) images. The arrows indicate (a, a*) crossroad areas 2 (green), band of migrating glial and neuronal cells (red), germinal matrix (orange), (b, b*) crossroad areas 5, (c, c*) von Monakow II segment, (d, d*) PLIC myelin (yellow), (e, e*) hippocampus and (f, f*) subplate compartments.

Statistical Analysis

A simple linear regression model was used to explain the relationship between standard HR images and reconstructed SR images. The variables were the volumes of the segmented structures. Furthermore, Dice similarity coefficients were computed between HR and SRR for each segmented brain region. A Wilcoxon Signed-Rank test was performed to compare fine structure visibility scores between standard HR and reconstructed SR images. All the statistical analyses were done on MATLAB.

Results

According to the quality assessments of standard T2w HR images (Table 1), across subjects' scans (n=113), 48% (54/113) of HR images were good, 22% (25/113) were medium and 30% (34/113) were poor quality (severely motion corrupted). The success rate to obtain a good quality HR image in the single scan was 39% (44/113), (FT=7% [8/113], PTB=11% [12/113], TEA=21% [24/113]) and in the second trial was 9% (10/113). 48% (11/23) of FT, 33% (15/45) of PTB and 62% (28/45) of TEA had good quality of HR images. Additionally, statistics of obtaining good quality of SRR images were 74% (26/35), 6% (2/35) medium and 20% (7/35) poor.

The phantom experiment showed a similarity structure index of SSIM=0.91 between HR and SRR images. Figure 4 and Figure 5 show the comparisons of LR images and reconstructed SR volumes of two neonatal subjects in orthogonal views. The red squares indicate coronal, sagittal, and axial acquired LR data in the first three columns. The last two columns show the initial estimation, which is the average of all registered LR images and SRR of the

orthogonal acquired LR images. In Figure 4, spatial resolution of LR was 0.6x0.6x2 mm^3 and SRR was 0.6 mm^3 isotropic whereas in Figure 5 spatial resolution of LR was 0.8x0.8x3 mm^3 and SRR was 0.8 mm^3 isotropic. The squares below the figures show magnified areas. The edges and lines are sharper and enhanced compared to the initial estimation.

In Figure 6, reconstructed super-resolution and standard high-resolution are represented for one subject. The hippocampus is well visible in both images. However, in the standard HR image, there are minor artifacts such as lines in the forehead and around corpus callosum (pointed by arrows) due to small movements. Figure 7A. shows histogram of the fine structure visibility scores of SRR and HR images (n=18 subjects, 8 structures). Fine structures of crossroad areas 2 and 5, Von Monakow, band of migrating glial and neuronal cells, germinal matrix and subplate compartments were mostly well visible on both HR and SRR images. Hippocampus had better score in HR whereas PLIC myelin had better scoring in SRR. Paired differences between SRR and HR scores (Figure 7B.) shows that the vast majority of the structures are viewed identically (bar b). The better performance of HR (bar a) is due to a better visibility of the hippocampus, whereas the better performance of SRR (bar c) is due to an improved visibility of PLIC in SRR. Wilcoxon Signed-Rank test result was p=0.63, Z=0.48. Therefore, the difference between HR and SRR images was not large enough to be statistically significant.

Figure 8 shows the comparison of morphology-based segmentation applied to standard HR image versus the SR reconstructed volume of one neonatal subject (red label: white matter, gray label: gray matter, blue label: CSF, white label: basal ganglia, green label: brain stem, yellow label: cerebellum). Figure 9 represents the linear regression plots of segmented HR and SRR volumes for each brain region. R^2values for gray matter, white matter, cerebrospinal fluid, basal ganglia, cerebellum and total volume including brain stem were 0.963, 0.973, 0.965, 0.970, 0.957, and 0.998, respectively. The average Dice similarity coefficients for GM, WM, CSF, BG, Crb, and BS brain regions were 0.85±0.02, 0.88±0.02, 0.83±0.04, 0.96±0.01, 0.91±0.02, and 0.92±0.01, respectively.

Discussion

We compared super-resolution reconstruction method to standard T2w high-resolution MRI for neonatal brain imaging. Acquiring HR images which are both good contrast and of high-quality is quite challenging in infants. Due to the fact that MRI is highly sensitive to motion, long acquisition times increase the likelihood of image degradation. In clinical settings, sedation (or general anesthesia) is commonly used to circumvent motion issues. In the research setting, sedation (or general anesthesia) is not an option due to ethical considerations. Supportive air pillows are often used to limit subject’s motion but cannot fully eliminate baby’s movements. Usually when the images have unacceptable motion artifacts, the sequence is reacquired, thus doubling the scan time.

The reacquisition of a motion corrupted scan does not guarantee a good quality image. In our study, we found that the success rate for obtaining a motion-free HR image in a single scan was 39% across all subjects; often subjects with severe motion artifacts were scanned 2-3 times to obtain good quality HR image (TA=5 min). However, the success rate of

obtaining good HR at the second trial was only 9% in total. In other words, 5 to 15 minutes of scan time is consumed to obtain an adequate structural image, with very limited chance of success. Considering the HR image quality success rates, 48% of the total subjects had good quality images. These findings are close to the reports of previous studies: a similar study found that no motion was evident on the T2w TSE images of 53% of the infants (n=132)[26] whereas another study on unsedated neonatal subjects reported that image quality of 52% was excellent, 46% were acceptable and 2% were poor or unacceptable (n=155).[27] In most of the trials where sedation or anesthesia is not given to the subject, most of the images have motion artifacts. These findings support the need of an alternative method to increase the success rate in newborn imaging.

Instead of lengthy 2D HR image acquisition we can acquire several fast LR images in different orientations and thicknesses (TA<min) and reconstruct them in 3D using super-resolution algorithms. In the case of subject motion, reacquisition time is short and even without any repetition, the rate of obtaining good quality of SRR image was improved (74%). The SRR method is efficient when applied to the thick LR slices, in order to reduce the anisotropy of the voxels. Low-resolution stacks can be acquired in two ways: through-plane LR shift and multiple orientation. However, our previous research has shown that multiple orientation acquisitions yield better SR reconstructions compared to through-plane shift acquisitions. SR reconstruction promises better resolution than standard HR image acquisition when SNR limitations and total scan time are considered.[13]

In this study, we reconstructed super-resolution volumes from mutually orthogonal and rapidly acquired low-resolution 2D T2-weighted neonatal MR images using multi-scale gradient field prior in combination with a MAP approach. Standard HR and reconstructed SR images from neonatal subjects (n=10, both high-quality HR and SRR) were segmented with a morphology-based segmentation method. Visual inspection and quantitative assessments showed very similar results for segmented volumes. Simple linear regression analysis indicated that there is a high correlation between standard HR acquisition and SR reconstruction. Each brain region volume had correlation results close to 1. In spite the fact that GM, WM and CSF are especially challenging to segment in the neonatal brain due to thin cortical thicknesses and the ongoing myelination process. Dice similarity coefficients for each brain region were computed to quantify the overlap between the segmentations of the two datasets. Dice coefficients for brain regions averaged from 0.83±0.04 (CSF), to 0.96±0.01 (BG), which are well above a value of 0.7 that considered as good overlap.[28] Overall, these results show that the SR reconstructed volume can equally be used for morphometrical purposes, without bias.

One of the key issues of SR reconstruction is the preservation of the contrast and edges which are critical for the assessment of cerebral maturation. We reviewed the detectability of fine structural landmarks whose visibility depends on the quality of the images in terms of resolution and contrast. These structures namely periventricular bands of migration, germinal matrix over the head of the caudate nucleus, crossroads 2 and 5, von Monakow segments II, linear subplate compartment along the Sylvian scissure, hippocampus and PLIC are all visible in both full-term and preterm infants. There was no sufficiently marked difference between HR and SRR image scorings to be statistically significant. Furthermore,

these structures could be equally well detected in SRR and HR images, except for the hippocampus and PLIC. The hippocampus was better visible on HR image (Figure 7b, bar A) due to the fact that HR was acquired in coronal plane which is the best plane for visualizing the folding of the hippocampus. The PLIC was best detected in SRR image (Figure 7b, bar C) thanks to the gain of resolution in the axial plane, which corresponds to the orientation that best visualizes PLIC bundle. The limitation of our study is the small number of subjects. It is challenging to obtain good quality SRR and HR datasets for comparison, in the constraint of total acquisition time.

As a conclusion, acquisition of multiple 2D T2w low-resolution images reduced the risk of motion artifacts. SR reconstruction of LR images resulted in good quality high-resolution volumes. SRR as presented in the results provided images with comparable structural information in terms of morphometry and diagnostic assessments compared to the standard T2 weighted HR image.

Acknowledgements and Disclosure

We would like to thank all the radiology technicians and neonatologists who helped us during data acquisition in University Hospitals of Geneva. We would like to acknowledge that authors have no financial conflicts-of-interest to disclosure. Conference abstract related the study: Askin NC, Gui Levy L, SaDeAlmeida J, Kocher M, Huppi P, Lazeyras F. Super-resolution reconstruction applied to neonatal MRI: orthogonal vs through-plane slice shift MRI acquisition and segmentation. In proceedings of 27th Annual Meeting of ISMRM. Montreal, QC, Canada2019:423.

Funding:

N.C.A.I. is supported by SNF Doc. Mobility Grant number P1GEP2_184160. S.K.W., O.A., T.E.W., and Y.S. are supported by NIH funding from R01 EB019483.

References

1. Huppi PS, Warfield S, Kikinis R, et al. Quantitative magnetic resonance imaging of brain development in premature and mature newborns. Ann Neurol 1998;43:224–35. [PubMed: 9485064]
2. Ferriero DM. Neonatal brain injury. N Engl J Med 2004;351:1985–95. [PubMed: 15525724]
3. Miller SP, Ferriero DM, Leonard C, et al. Early brain injury in premature newborns detected with magnetic resonance imaging is associated with adverse early neurodevelopmental outcome. J Pediatr 2005;147:609–16. [PubMed: 16291350]
4. Huppi PS, Inder TE. Magnetic resonance techniques in the evaluation of the perinatal brain: recent advances and future directions. Semin Neonatol 2001;6:195–210. [PubMed: 11483024]
5. Prayer D, Kasprian G, Krampl E, et al. MRI of normal fetal brain development. Eur J Radiol 2006;57:199–216. [PubMed: 16413984]
6. Judas M, Rados M, Jovanov-Milosevic N, Hrabac P, Stern-Padovan R, Kostovic I. Structural, immunocytochemical, and mr imaging properties of periventricular crossroads of growing cortical pathways in preterm infants. AJNR Am J Neuroradiol 2005;26:2671–84. [PubMed: 16286422]
7. Sadeghi N, Prastawa M, Fletcher PT, Wolff J, Gilmore JH, Gerig G. Regional characterization of longitudinal DT-MRI to study white matter maturation of the early developing brain. Neuroimage 2013;68:236–47. [PubMed: 23235270]
8. Gui L, Lisowski R, Faundez T, Huppi PS, Lazeyras F, Kocher M. Morphology-driven automatic segmentation of MR images of the neonatal brain. Med Image Anal 2012;16:1565–79. [PubMed: 22921305]
9. Hennig J. K-space sampling strategies. Eur Radiol 1999;9:1020–31. [PubMed: 10415232]
10. Hamilton J, Franson D, Seiberlich N. Recent advances in parallel imaging for MRI. Prog Nucl Magn Reson Spectrosc 2017;101:71–95. [PubMed: 28844222]

11. Kim K, Habas PA, Rousseau F, Glenn OA, Barkovich AJ, Studholme C. Intersection based motion correction of multislice MRI for 3-D in utero fetal brain image formation. IEEE Trans Med Imaging 2010;29:146–58. [PubMed: 19744911]
12. Park SC, Park MK, Kang MG. Super-resolution image reconstruction: A technical overview. Ieee Signal Processing Magazine 2003;20:21–36.
13. Van Reeth E, Tham IWK, Tan CH, Poh CL. Super-resolution in magnetic resonance imaging: A review. Concepts in magnetic resonance part A 2012;40A:306–25.
14. Plenge E, Poot DHJ, Bernsen M, et al. Super-resolution methods in MRI: Can they improve the trade-off between resolution, signal-to-noise ratio, and acquisition time? Magn Reson Med 2012;68:1983–93. [PubMed: 22298247]
15. Jiang S, Xue H, Glover A, Rutherford M, Rueckert D, Hajnal JV. MRI of moving subjects using multislice snapshot images with volume reconstruction (SVR): application to fetal, neonatal, and adult brain studies. IEEE Trans Med Imaging 2007;26:967–80. [PubMed: 17649910]
16. Rousseau F, Glenn O, Iordanova B, et al. A novel approach to high resolution fetal brain MR imaging. Med Image Comput Comput Assist Interv 2005;8:548–55. [PubMed: 16685889]
17. Gholipour A, Estroff JA, Sahin M, Prabhu SP, Warfield SK. Maximum a posteriori estimation of isotropic high-resolution volumetric MRI from orthogonal thick-slice scans. Med Image Comput Comput Assist Interv 2010;13:109–16. [PubMed: 20879305]
18. Gholipour A, Estroff JA, Warfield SK. Robust super-resolution volume reconstruction from slice acquisitions: application to fetal brain MRI. IEEE Trans Med Imaging 2010;29:1739–58. [PubMed: 20529730]
19. Kuklisova-Murgasova M, Quaghebeur G, Rutherford MA, Hajnal JV, Schnabel JA. Reconstruction of fetal brain MRI with intensity matching and complete outlier removal. Med Image Anal 2012;16:1550–64. [PubMed: 22939612]
20. Tourbier S, Bresson X, Hagmann P, Thiran JP, Meuli R, Cuadra MB. An efficient total variation algorithm for super-resolution in fetal brain MRI with adaptive regularization. Neuroimage 2015;118:584–97. [PubMed: 26072252]
21. Sui Y, Afacan O, Gholipour A, Warfield SK. Isotropic MRI super-resolution reconstruction with multi-scale gradient field prior. In: Shen D, ed. Medical Image Computing and Computer Assisted Intervention – MICCAI 2019: Springer, Cham; 2019.
22. Greenspan H, Oz G, Kiryati N, Peled S. MRI inter-slice reconstruction using super-resolution. Magn Reson Imaging 2002;20:437–46. [PubMed: 12206870]
23. Akhondi-Asl A, Afacan O, Balasubramanian M, Mulkern RV, Warfield SK. Fast myelin water fraction estimation using 2D multislice CPMG. Magn Reson Med 2016;76:1301–13. [PubMed: 26536382]
24. Mattes D, Haynor D, Vesselle H, Lewellyn T, Eubank W. Nonrigid multimodality image registration: SPIE; 2001.
25. Pittet MP, Vasung L, Huppi PS, Merlini L. Newborns and preterm infants at term equivalent age: A semi-quantitative assessment of cerebral maturity. Neuroimage Clin 2019;24:102014. [PubMed: 31683202]
26. Hughes EJ, Winchman T, Padormo F, et al. A dedicated neonatal brain imaging system. Magn Reson Med 2017;78:794–804. [PubMed: 27643791]
27. Haney B, Reavey D, Atchison L, et al. Magnetic resonance imaging studies without sedation in the neonatal intensive care unit: safe and efficient. J Perinat Neonatal Nurs 2010;24:256–66. [PubMed: 20697244]
28. Zijdenbos AP, Dawant BM, Margolin RA, Palmer AC. Morphometric analysis of white-matter lesions in MR-images - method and validation. IEEE Trans Med Imaging 1994;13:716–24. [PubMed: 18218550]

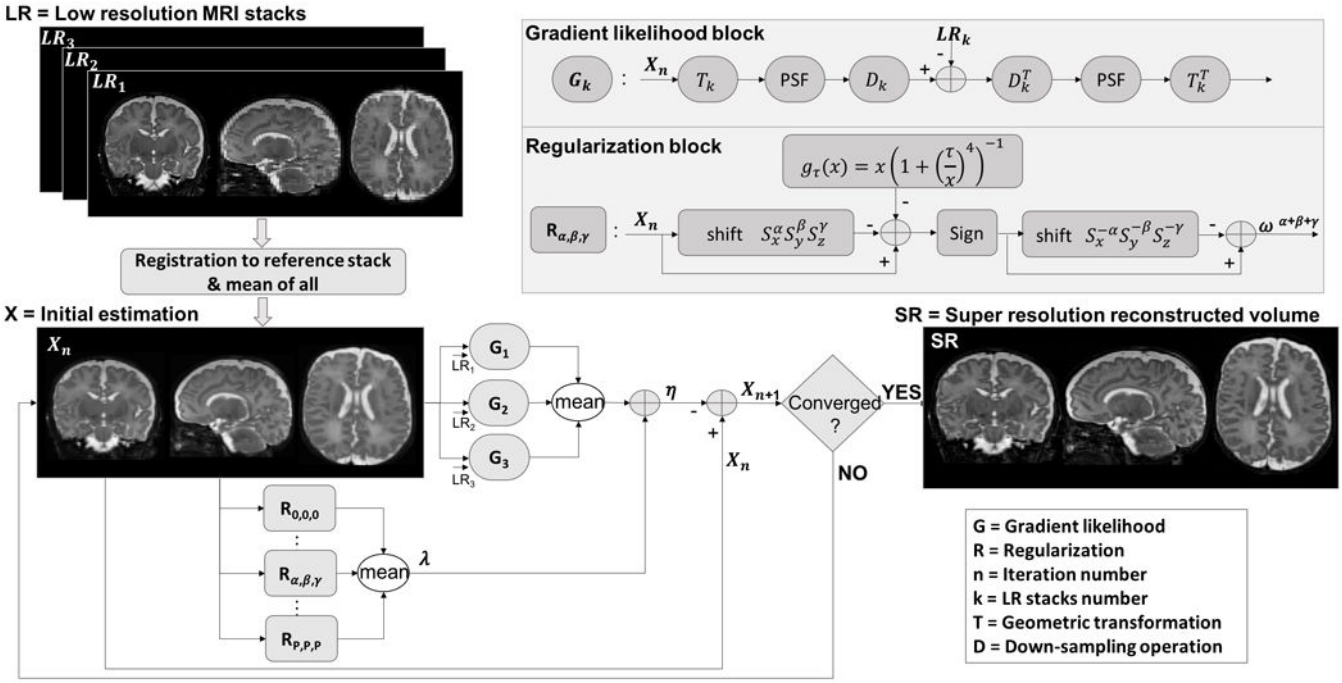

Figure 1.
Flowchart of the super-resolution reconstruction algorithm (PSF: Point spread function)

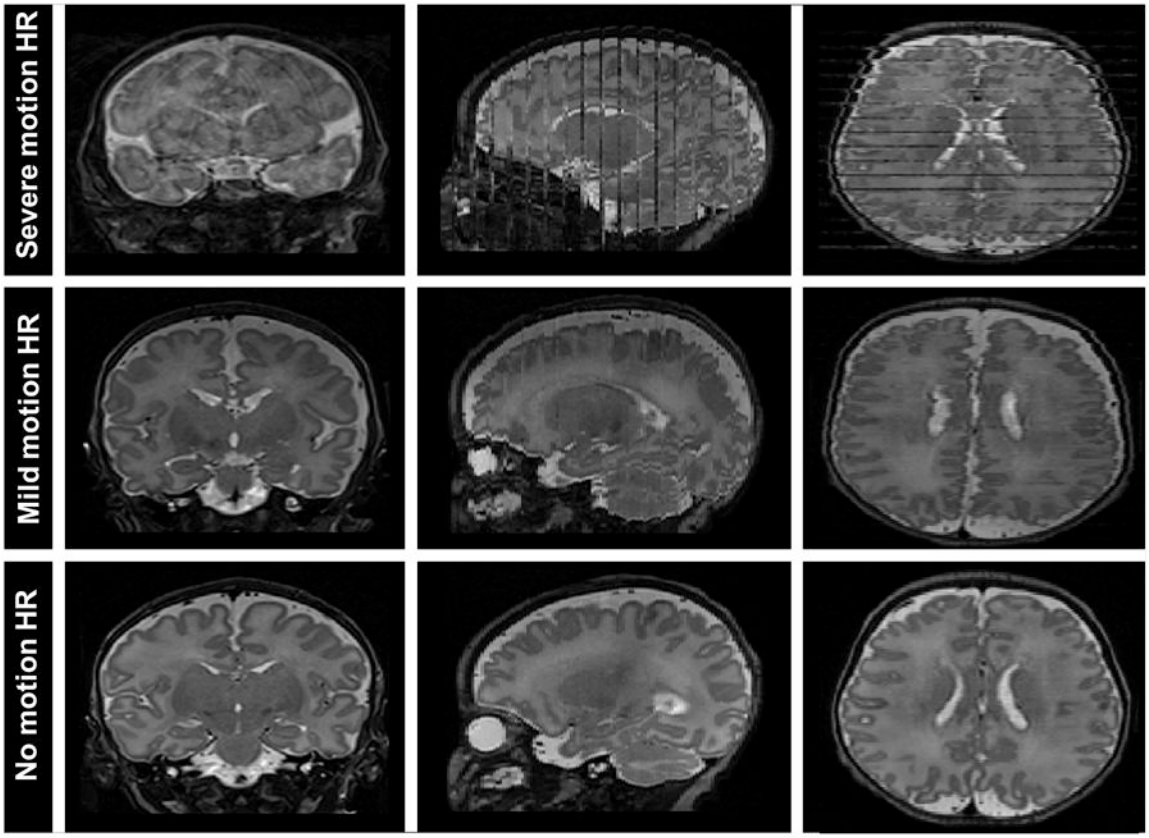

Figure 2.

2D T2-weighted high-resolution (HR) MR images of three neonatal subjects. In the top row, there are severe motion artifacts on the images whereas in the second row, that subject has only mild motion. The bottom row is an example of a high-quality standard HR image.

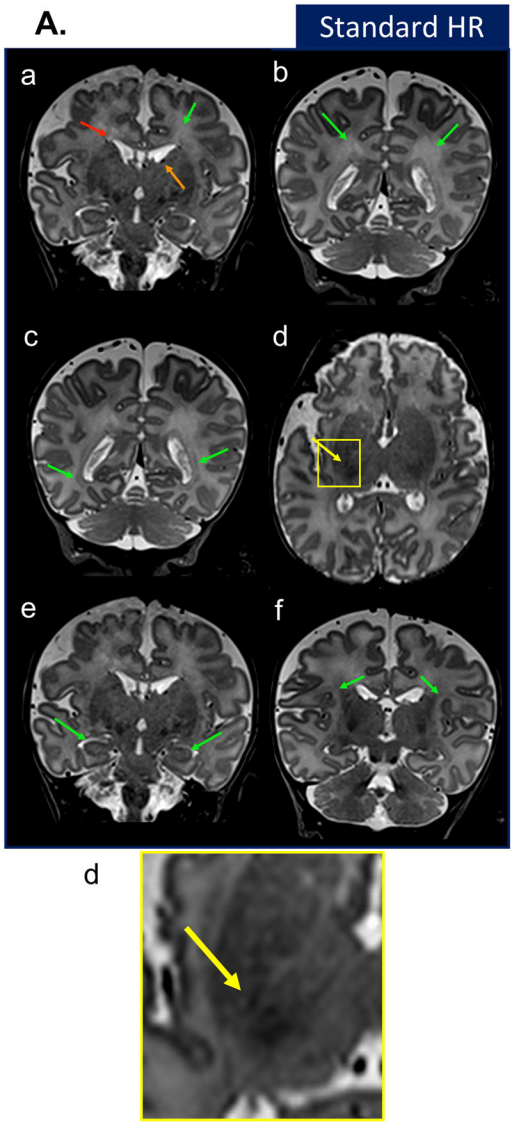

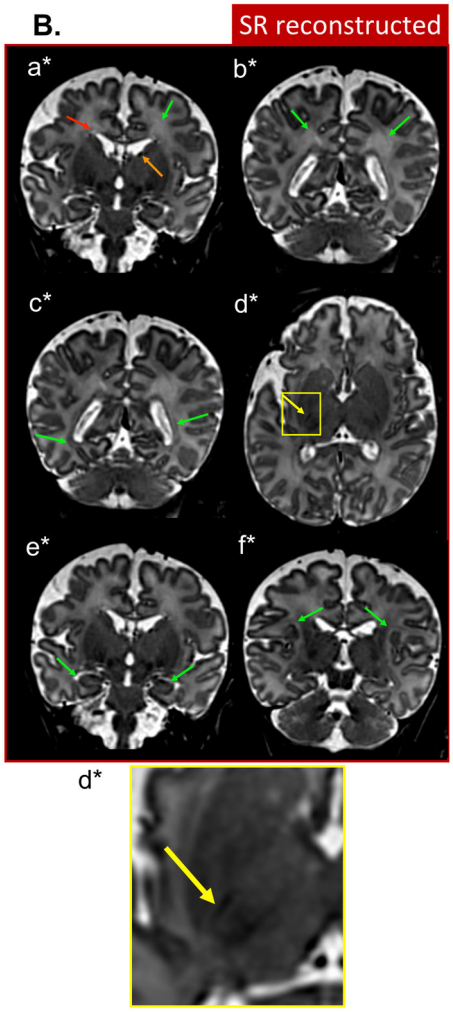

Figure 3.

Anatomical landmarks visibility comparison between high-resolution (HR) scans (Fig3A) and super-resolution (SR) reconstructed images (Fig3B). The arrows indicate (a, a*) crossroad areas 2 (green), band of migrating glial and neuronal cells (red), germinal matrix (orange), (b, b*) crossroad areas 5, (c, c*) von Monakow II segments, (d, d*) Posterior limb of the internal capsule myelin (yellow), (e, e*) hippocampus and (f, f*) subplate compartments according to Pittet et al.[25] These slices were chosen to best show structures of a newborn. Only the figures on (d, d*) displayed in axial view, the rest were shown in coronal view.

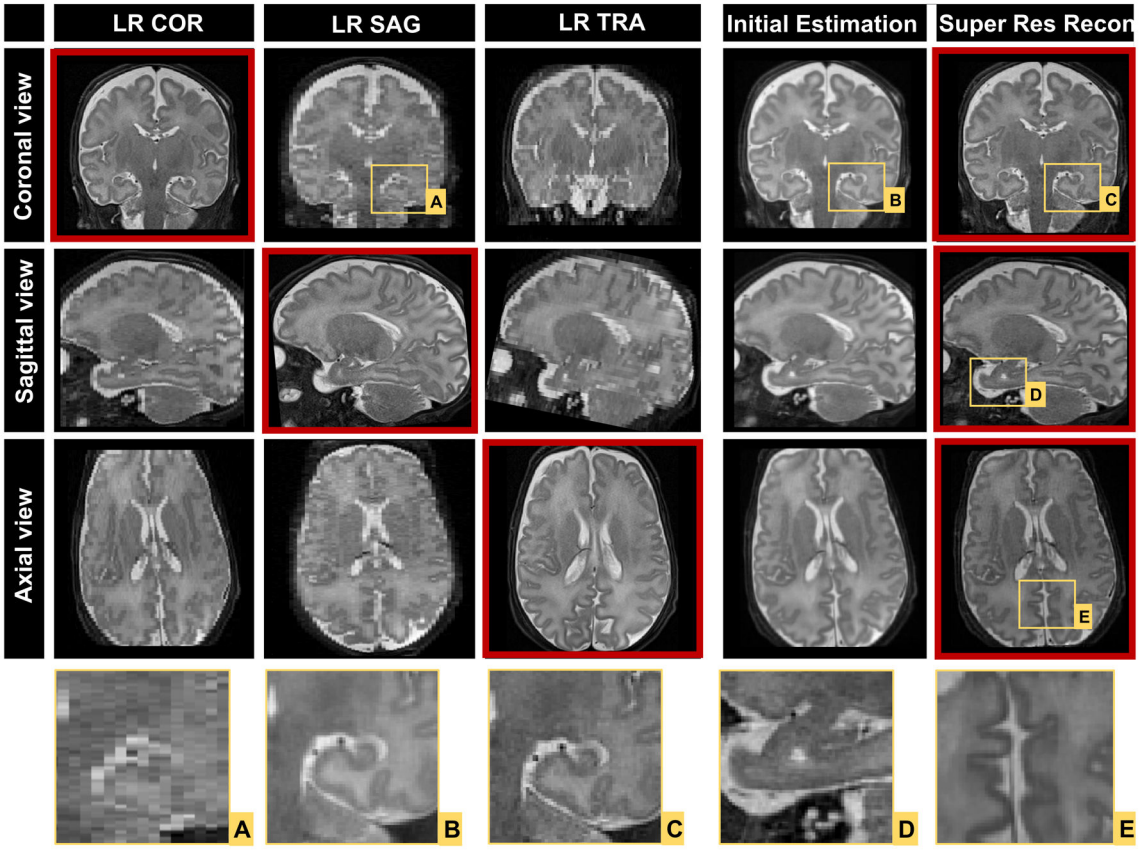

Figure 4.

Acquired low-resolution (LR) images compared with super-resolution reconstructed volume from three LR images which is yielding 0.6 mm^3 isotropic spatial resolution. (COR: coronal, SAG: sagittal and TRA: transversal view, Res: Resolution)

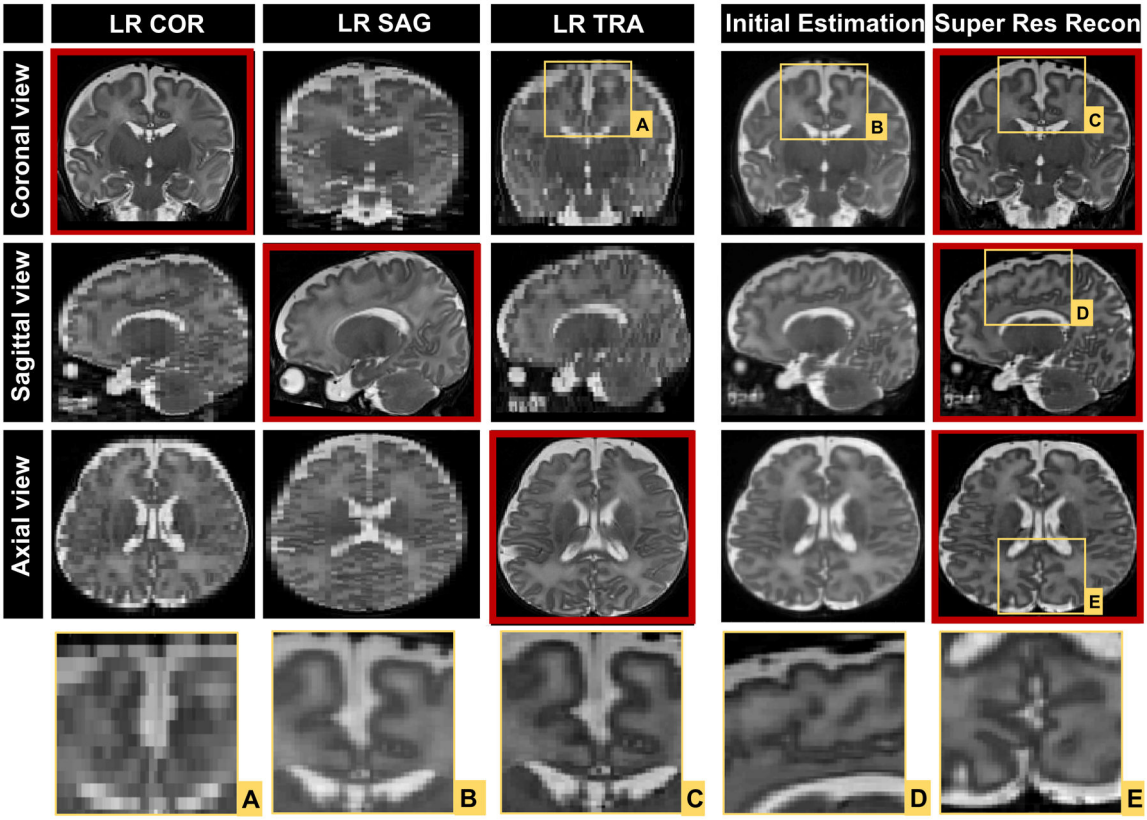

Figure 5.

Acquired low-resolution (LR) images compared with super-resolution reconstructed volume from three LR images which is yielding 0.8 mm^3 isotropic spatial resolution. (COR: coronal, SAG: sagittal and TRA: transversal view, Res: Resolution)

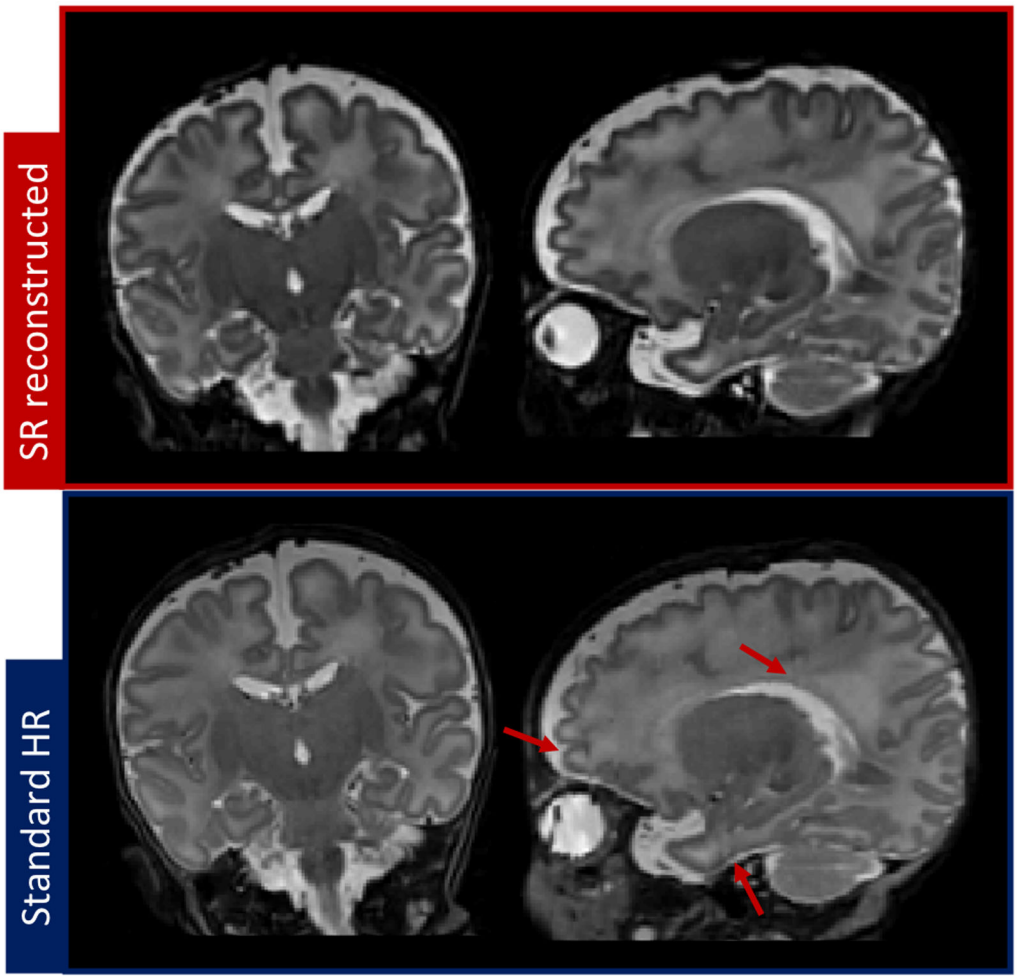

Figure 6.
Standard high-resolution (HR) versus super-resolution reconstructed image of one subject. The arrows point minor artifacts on HR image.

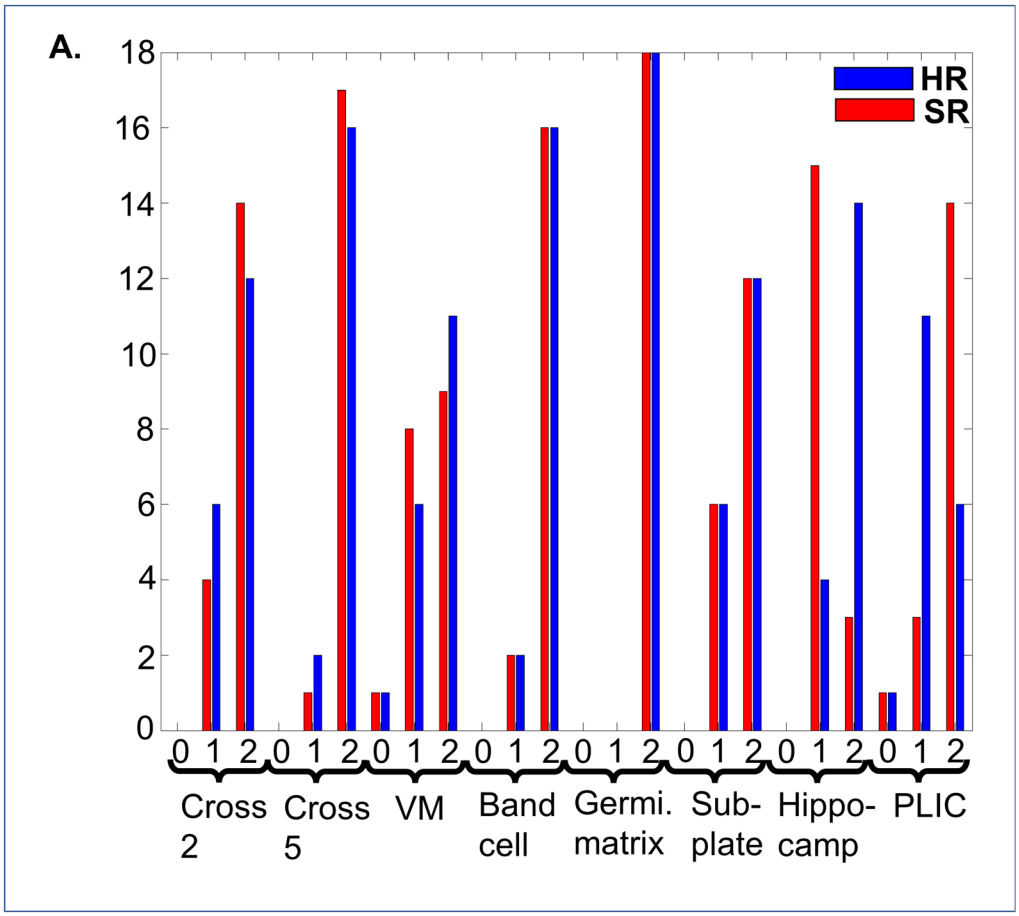

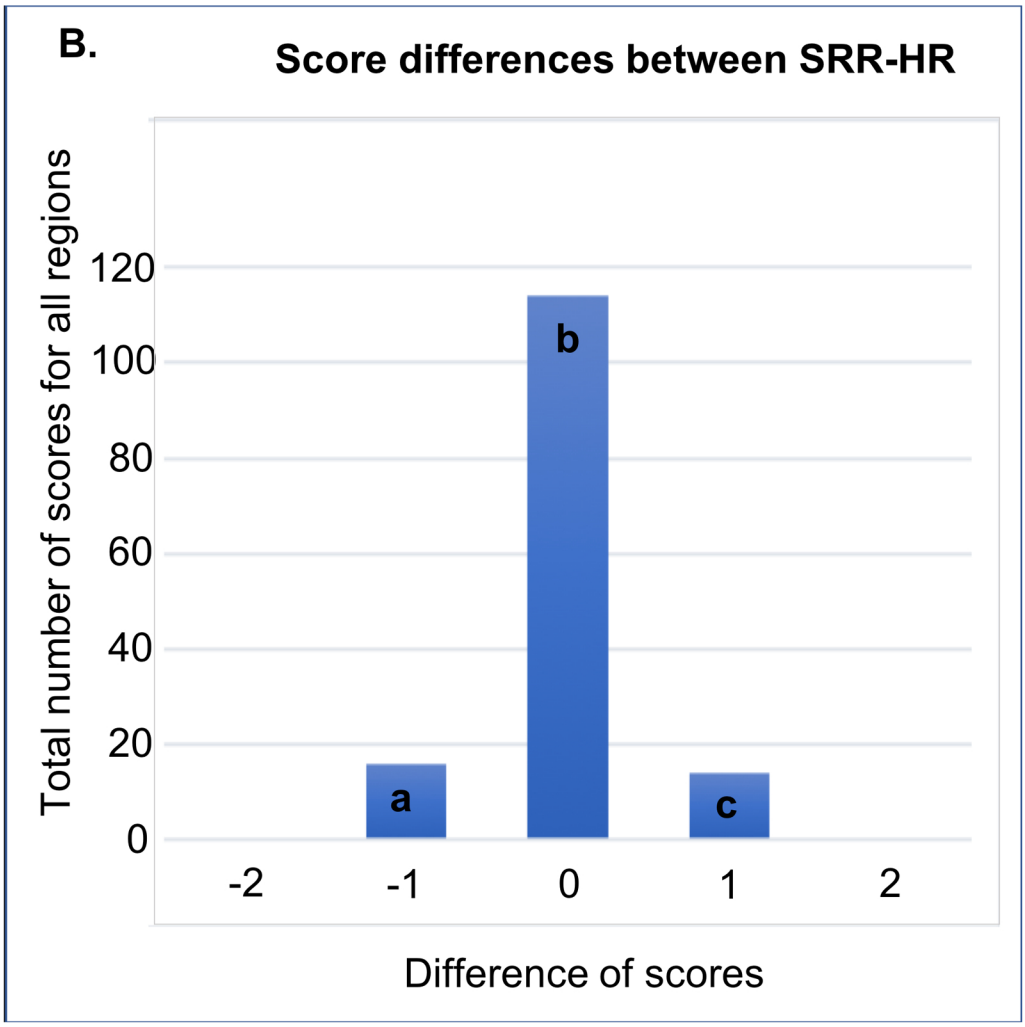

Figure 7.

(A.) shows the visibility scores (0 not visible, 1 visible with limitation, 2 is well visible) of the fine structures in super resolution reconstructed (SRR, labeled in red) and high resolution (HR, labeled in blue) images of each neonate (18 subjects, 8 structures) and (B.) shows the paired differences of the scores between SRR and HR images (SRR-HR, all regions included). Hippocampus for instance is better visible in HR whereas PLIC is better visible in SRR images. These differences correspond to bar a and c, respectively. (VM: von Monakow II, PLIC: Posterior limb of the internal capsule)

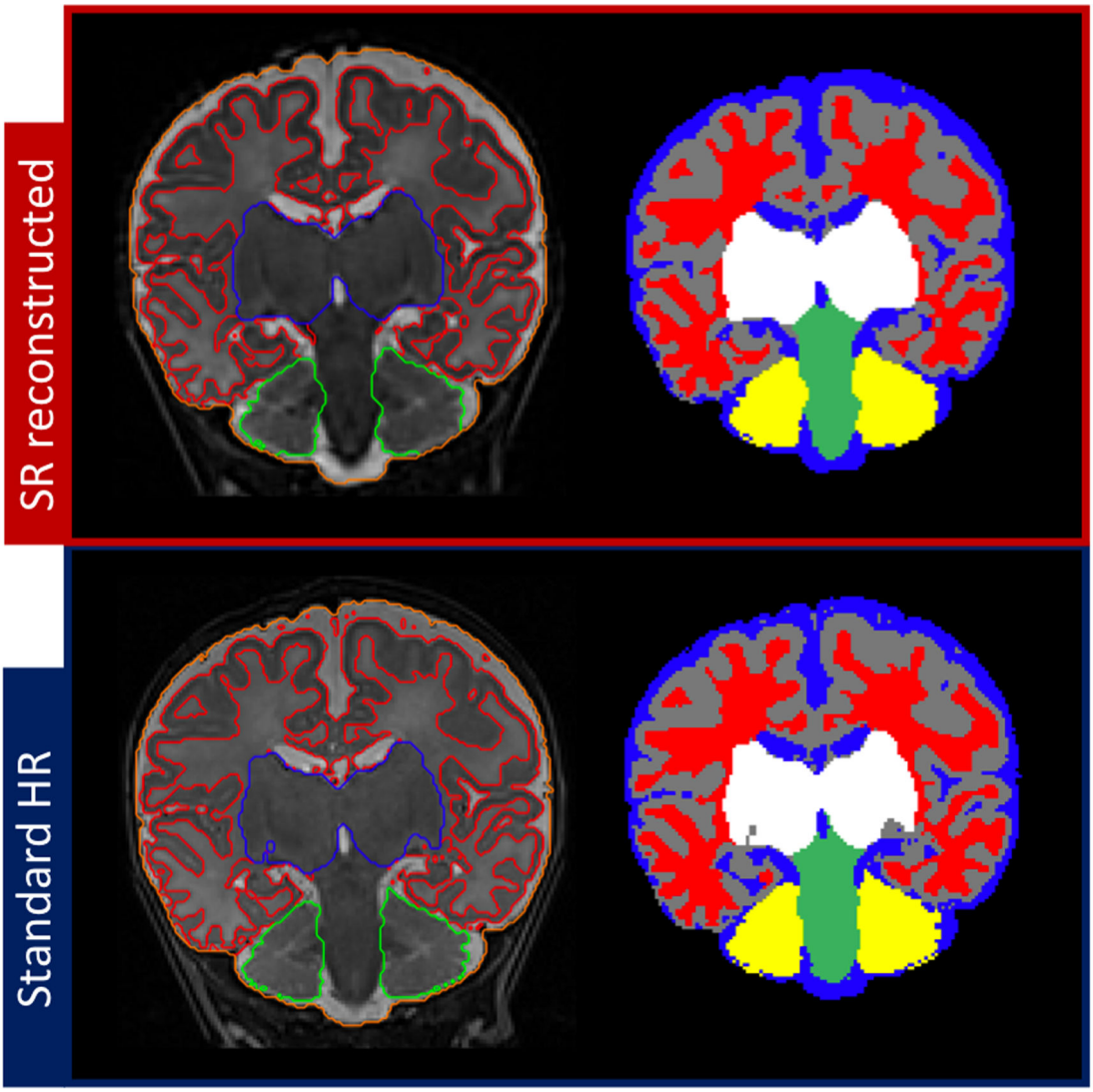

Figure 8.

Compared segmentations of standard 2D high-resolution image versus super-resolution reconstructed 3D volume of one subject (labels in red: white matter, gray: gray matter, blue: cerebrospinal fluid, white: basal ganglia, green: brain stem, yellow: cerebellum)

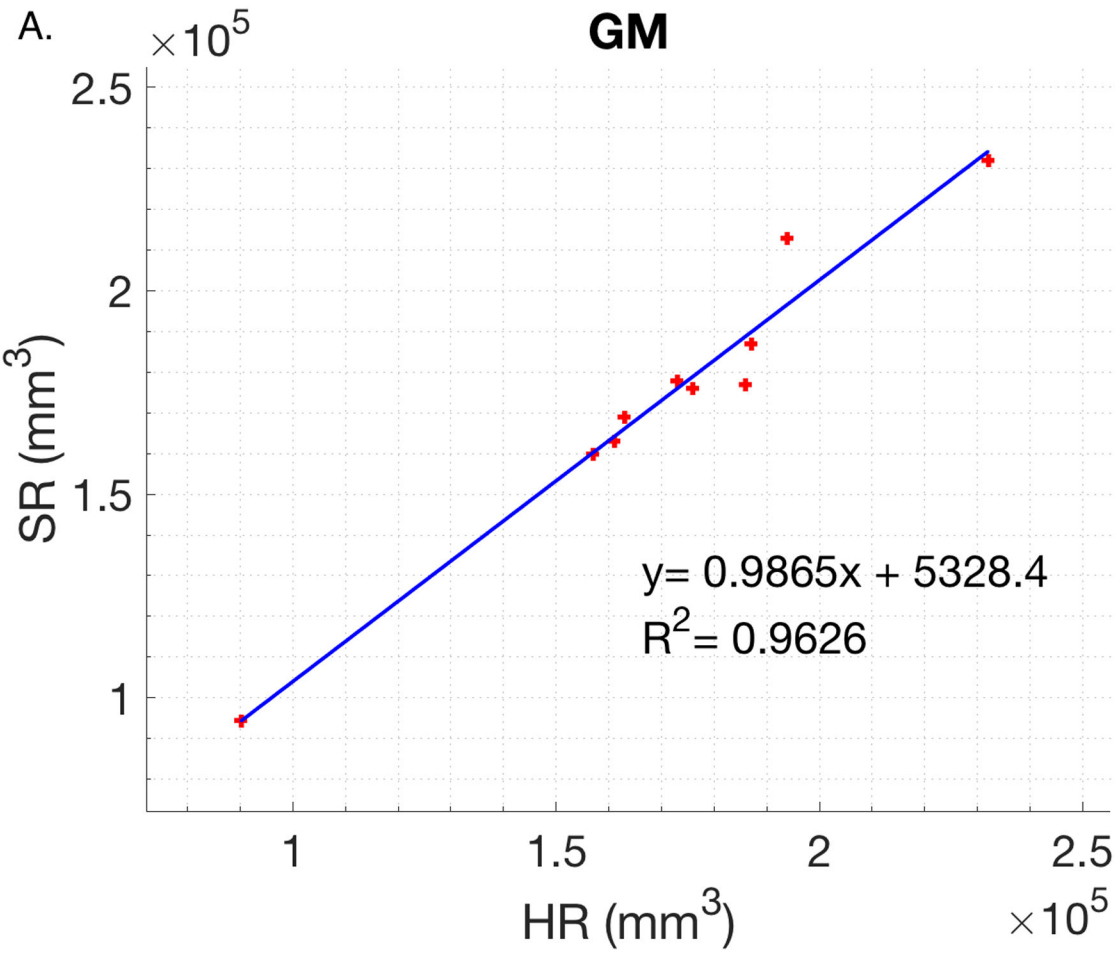

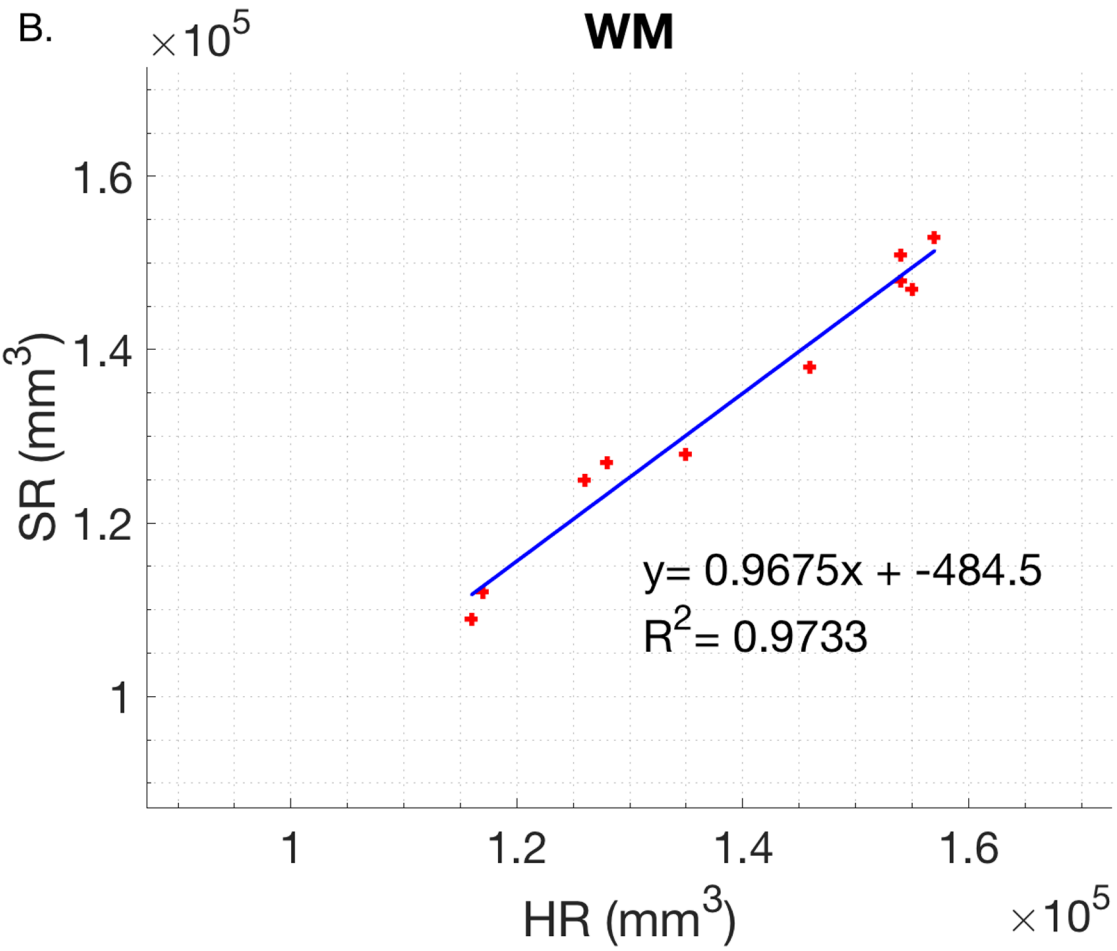

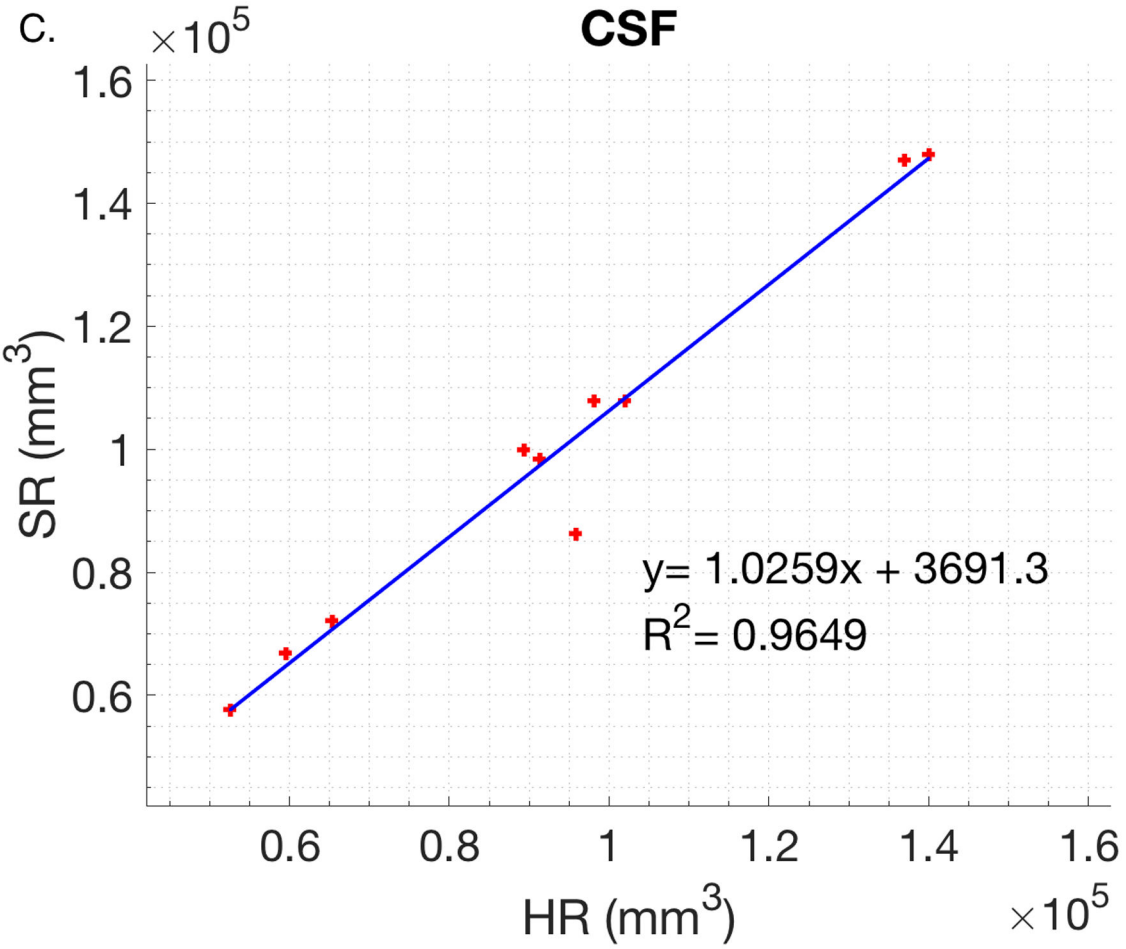

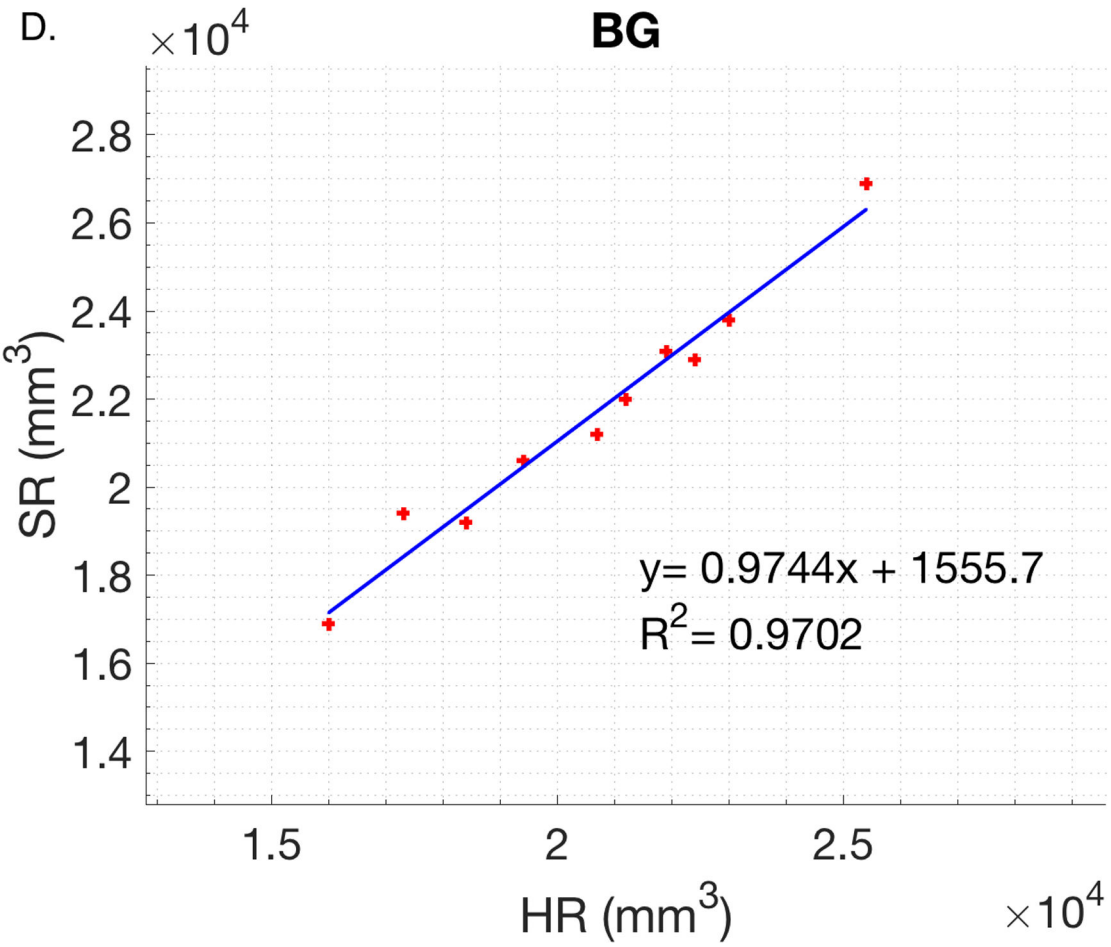

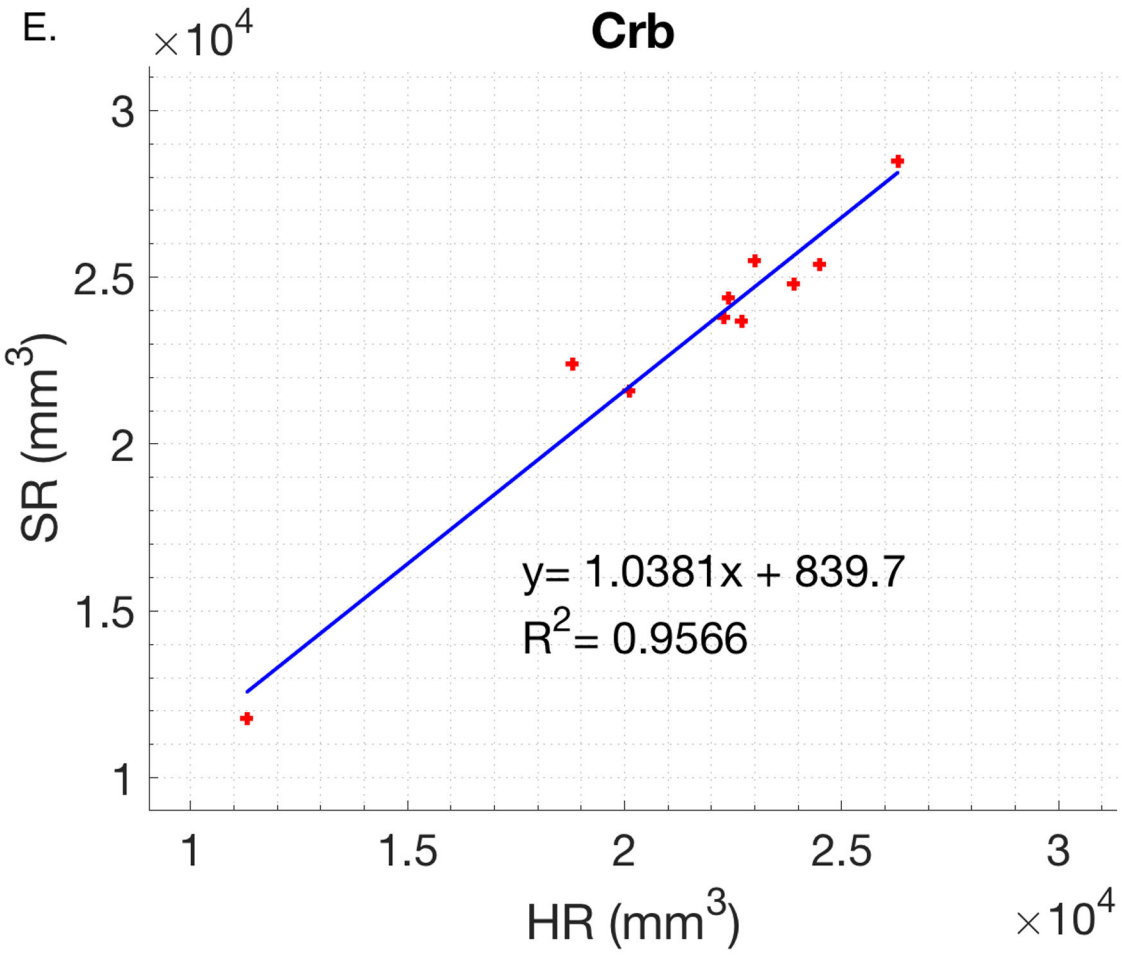

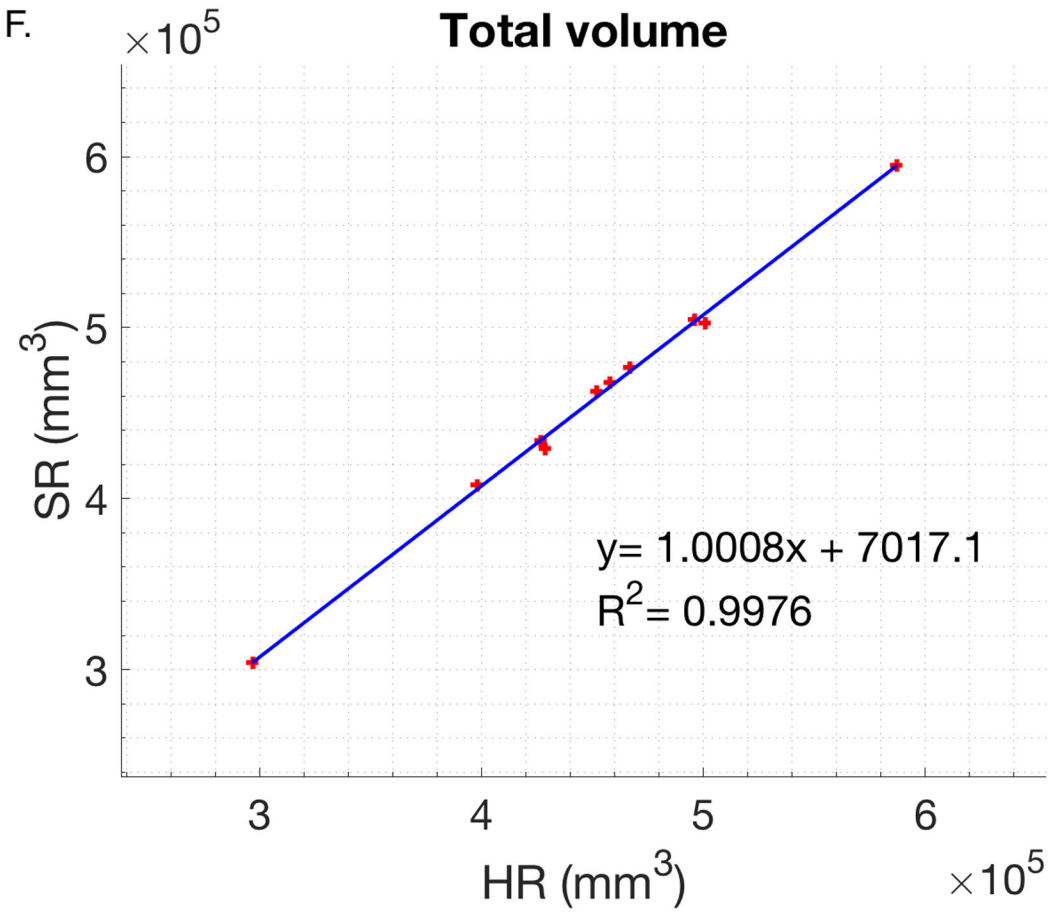

Figure 9.

Linear regression plots for segmented super-resolution reconstruction and high-resolution images of each region (GM: gray matter, WM: white matter, CSF: cerebrospinal fluid, BG: basal ganglia, Crb: cerebellum) and total brain volume including brain stem.

Table 1.

The table shows image quality assessments on standard 2D T2 weighted high-resolution images and success rates on single scan and reacquisitions for each group of subjects (full-term, preterm at birth and term equivalent age).

		Quality Assesment of HR Images (%)			Success Rate for Good Quality Acquisition (%)	
Subjects	**n**	**Good**	**Medium**	**Poor**	**Single Scan**	**2nd repeat**
FT	23	48	39	13	35	13
PTB	45	33	29	38	26	7
TEA	45	62	7	31	53	9
Total	113	48	22	30	39	9

FT:Full-term, PTB: Preterm at birth and TEA:Term equivalent age, HR: High-resolution, n: number of scans